

Autonomous Inversion of In Situ Deformation Measurement Data for CO₂ Storage Decision Support

J. Burghardt^{a,*}, T. Bao^a, K. Xu^c, A. Tartakovsky^b, E. Darve^c

^a*Pacific Northwest National Laboratory, Richland, Washington; USA*

^b*University of Illinois Urbana-Champaign, Urbana-Champaign, Illinois; USA*

^c*Stanford University, Stanford, California; USA*

Abstract

Geologic carbon storage (GCS) is likely to play a key part of the global effort to dramatically reduce CO₂ emissions and perhaps even reduce atmospheric CO₂ concentrations through carbon negative operations. A critical part of effort to commercialize and widely deploy this technology is developing the capability to rapidly assimilate real-time monitoring data into a form that will enable site operators to make decisions to manage the safe and efficient operations. Two of the risks associate with GCS are the risk of inducing fractures in the sealing formations that can create leakage pathways and the risk of inducing earthquakes of sufficient magnitude to cause public concern, property damage, or safety risks. To properly manage these risks the site operator needs to know the initial state of stress, the change in stress induced by injection, and the relationship between operational parameters such as injection rate and pressure and the change in stress. Current methods of estimating the change in stress require choosing the type of constitutive model and the model parameters based on core, log, and geophysical data during the characterization phase, with little feedback from operational observations to validate or refine these choices. These characterization methods interrogate the geologic formations using length scales, loading rates or magnitudes that are quite different from those encountered by the actual storage system. It is shown that errors in the assumed constitutive response, even when informed by laboratory tests on core samples, are likely to be common, large, and underestimate the magnitude of stress change caused by injection. Recent advances in borehole-based strain instruments and borehole and surface-based tilt and displacement instruments have now enabled monitoring of the deformation of the storage system throughout its operational lifespan. This data can enable validation and refinement of the knowledge of the geomechanical properties and state of the system, but brings with it a challenge to transform the raw data into actionable knowledge. We demonstrate a method that uses automatic differentiation and a finite-element based geomechanical model perform a gradient-based deterministic inversion of geomechanical monitoring data. This

*Corresponding author

Email address: jeffrey.burghardt@pnnl.gov (J. Burghardt)

approach allows autonomous integration of the instrument data without the need for time consuming manual interpretation and selection of updated model parameters. Furthermore, only isotropic linear elasticity is considered in this paper, the approach presented is very flexible as to what type of geomechanical constitutive response can be used. The approach is easily adaptable to nonlinear physics-based constitutive models to account for common rock behaviors such as creep and plasticity. The approach also enables training of machine learning-based constitutive models by allowing back propagation of errors through the finite element calculations. This enables strongly enforcing known physics, such as conservation of momentum and continuity, while allowing data-driven models to learn the truly unknown physics such as the constitutive or petrophysical responses.

Keywords: geologic carbon storage, induced seismicity, hydraulic fracturing, finite element, geomechanics

1. Introduction

Geologic carbon storage increases the pore fluid pressure and consequently induces a deformation of the geologic strata. This deformation extends well beyond the storage formation itself, and usually extends beyond the upper and lower confining units. These deformations pose several risks that a site operator must consider and manage. The two most significant of these geomechanical risks are the risk of unintentionally inducing shear or tensile fractures that compromise the integrity of the sealing formations, and the risk of inducing earthquakes of sufficient magnitude to cause public concern, property damage, or safety risks. To properly manage these risks a site operator needs to understand both the initial state of stress of the system, and the changes in stress that are induced by storage operations. Traditional approaches to characterizing the change in the system use physics-based numerical geomechanical models. These are most commonly a finite-element based model that is coupled in some manner to a reservoir model that predicts the changes in fluid pressure caused by injection.

A numerical geomechanical model most commonly solves the governing equations for poroelastic continua. Some of these governing equations are very well understood and well validated, such as conservation of momentum, energy, and continuity. Unlike these well-known physical laws that apply universally to all spatial locations, a geomechanical analysis requires definition of a constitutive law that describes the relationship between stress, pore pressure, and deformation in each part of the domain being modeled. This relationship is not known a priori but must be chosen for every spatial location at each site. Characterizing this constitutive relationship, together with learning the initial conditions, are the two key geomechanical challenges and sources of uncertainty in accurately estimating changes in stress, strain, and displacement that drive geomechanical risk. This work will focus on a new method of learning the constitutive

relationship and leave the learning of the initial conditions out of the present discussion.

First, we will address the question of what effect inaccuracies in the constitutive relationship are likely to have on the practical operation of a GCS site. When the pore pressure increases because of CO₂ injection this causes a decrease (i.e. becomes less compressive) in the effective stress experienced by the rock itself. This decrease in effective stress causes a volumetric expansion of the pressurized rock. As one part of the subsurface expands adjacent sections must also deform to accommodate this deformation. This will cause some regions to compress and others to stretch. This deformation and the associated change in stress is what is responsible for the geomechanical risks of induced seismicity and the possibility of leakage through induced or activated fractures. In general, the larger the magnitude of these stress changes, the greater the geomechanical risk. Burghardt [4] used a tightly-coupled reservoir/geomechanical model to compare two scenarios: one where the ratio of cap rock shear modulus to reservoir shear modulus is 1.41, and one where this ratio is 0.44. The results from that analysis showed that the more compliant cap rock produces a change in stress that is approximately 50% greater than for the stiff cap rock case, which would indicate a much higher geomechanical risk.

The example given above shows that a significant error in the shear modulus estimate for the cap rock can lead to very large errors in the geomechanical risk prediction. The next question to address is whether such large errors in rock compliance are likely using existing approaches. To minimize the time, cost, and complexity, the most common characterization approaches assume a priori the simplest possible constitutive relationship, usually isotropic linear elasticity. This greatly simplifies the characterization problem, reducing the problem to estimation of two elastic moduli (e.g. Young's modulus and Poisson's ratio) that can be easily measured on core samples and correlated with log and seismic responses. However, by forcing the complex behavior of real subsurface systems into convenient linear models, a limit is placed on the fidelity to which the model can capture the reality of the subsurface processes.

Sone and Zoback [11] conducted a series of tests to characterize the difference between the deformation of US shale gas rocks during typical short-term laboratory tests and two-week long tests. Their results showed that even after two weeks of constant loading the samples were continuing to deform. The time-dependent strain appeared to be following a logarithmic or power-law type of response where the creep continues indefinitely at a decreasing rate. Extrapolation using an assumed power law trend showed that after one year the strain due to creep can reach 2.5 times that that occurs due to the instantaneous elastic deformation. To give a concrete example, if a sample of the Eagle Ford shale were tested in the laboratory using ISRM suggested methods, a 10 MPa applied stress would produce a strain of 0.4 millistrains, and result in a Young's modulus of 25 GPa. If the same sample were held under the same load for 1 year, using the creep compliance parameters estimated by Sone and Zoback [11], the measured strain would be 1.4 millistrains and the resulting Young's modulus would be 6.8 GPa. A ten-year long test, which would be representative of the

duration of injection of a typical GCS site, would show an even lower Young’s modulus of 5.7 GPa. In other words, the short-term test that is almost universally used today would overestimate the stiffness of the shale sample by 365% compared to how it would respond during the long-term stress changes occurring during CO₂ injection. This large error in the constitutive response would result in a very large underestimation of the stress change and corresponding geomechanical risk.

The results cited above show that errors in the constitutive relationship current approaches are likely to be large (up to several hundred percent), are not conservative (i.e. under-estimate risk), and to have important consequences for the estimation and management of geomechanical risk. A better estimation of the real constitutive response using current state of the art methods, as employed by Sone and Zoback [11] would result in an increased characterization cost of several orders of magnitude beyond what is common today since laboratory tests that take approximately 15 minutes today would be replaced with tests that take several hours or even weeks. Additionally, there is reason to think that the estimate given above are underestimates of the problem since core-scale tests do not capture larger scale features such as natural fractures and lithologic contacts that are additional sources of compliance and creep.

Instead we propose using in situ geomechanical monitoring instrumentation to update numerical geomechanical models throughout the lifespan of an injection site. This is analogous to traditional history matching approaches that use used to update the hydraulic properties of a reservoir using injection and production data. Murdoch et al. [9] recently summarized recent advances in geomechanical instrumentation and demonstrated that instruments are now available that can reliably resolve strains as small as one nano-strain. Additionally, recent results from laboratory [3] and field tests [12] show that fiber-optic distributed acoustic sensing (DAS) measurements may be capable of detecting very small magnitude strains, though extracting quantitative quasi-static strains from DAS data is an ongoing research effort. Even though some uncertainty remains about which strain sensing approach will prove to be optimal considering trade offs of accuracy, cost, and long-term reliability, it seems quite clear that data describing the deformation of subsurface storage systems will soon be available to operators. The challenge that remains is how to efficiently process this data in such a way that a site operator can use to make operational decisions.

2. Method

This section discusses the details of how a finite element method is used to solve the inverse problem of estimating constitutive model parameters using in situ geomechanical measurements. The method consists of beginning with an initial estimate for the constitutive model parameters and running standard finite element calculations to predict the monitoring instrument responses. Errors between the simulated and predicted response are quantified using a scalar loss function. The gradient of the loss function with respect to the constitutive model parameters is then computed by back propagation through the finite

element model. Then, using the loss function value and the its gradient with respect to the inversion parameters, a quasi-Newton optimization algorithm can be used to solve for the inversion parameters.

2.1. Back propagation through finite element calculations

A poromechanical finite element solver applies Newton-Raphson iteration to find the nodal displacements, u_i , that satisfy static equilibrium given body loads created by gravity and pore fluid pressure, constitutive parameters, and boundary conditions. The finite element approximation to the displacement field is constructed in such a way that the continuity is automatically satisfied. The expression for the vector of nodal residuals to the static equilibrium equation is

$$r(u_i, \theta_j) = \sum_{e=1}^{N_e} \int_{\Omega_e} [B(x)]^T \cdot \sigma'(u_i, \theta) dV_e - \int_{\Omega_e} [B(x)]^T \cdot \alpha \delta P_p dV_e + \int_{\Omega_e} \rho g [N(x)] dV_e \quad (1)$$

where N_e is the number of elements, $[B]$ is the strain-displacement matrix for each element, σ' is the Mandel effective stress tensor, θ is a set of constitutive model parameters, α is the Biot coefficient, P_p is the pore fluid pressure, ρ is the mass density, g is the acceleration due to gravity, and $[N]$ is the shape function matrix for each element. Note that the effective stress is a function of both the nodal displacements and a set of constitutive parameters. As will be explained below, these parameters may be traditional physics-based parameters such a Young's modulus, creep compliance, yield strength, etc., or they may be weights and biases in a deep learning model, or a combination of the two. The Newton-Raphson iteration proceeds using the iteration formula

$$\{u^{k+1}\} = \{u^k\} - [J_u]^{-1} \{r^k\} \quad (2)$$

Where k is the iteration number, and $[J_u]$ is the Jacobian matrix given by

$$J_u = \frac{\partial r(u_i, \theta)}{\partial u_j} = \sum_{e=1}^{N_e} \int_{\Omega_e} [B(x)]^T \cdot \left[\frac{\partial \Delta \sigma'(\theta)}{\partial \Delta \epsilon} \right] dV_e. \quad (3)$$

If a set of measurements of the deformation field induced by injection, d^i , are available, we can define a loss function, L , that quantifies the degree to which the finite element solution agrees with the measured response using an L_2 norm

$$L = \sum_{t=0}^p \sum_{i=0}^m \left[\frac{d_{\text{meas}}^i - d_{\text{pred}}^i(t, u, \theta)}{S_i} \right]^2 \quad (4)$$

where p is the number of time steps and m is the number of measurements incorporated into the loss function, and S_i is a scaling factor for each measurement. The gradient of the loss function with respect to the constitutive parameters can be expressed as

$$\begin{aligned} \frac{\partial L}{\partial \theta} &= \frac{\partial L}{\partial d_{\text{pred}}} \frac{\partial d_{\text{pred}}}{\partial u} \frac{\partial u}{\partial \theta} \\ &= [L][M][G] \end{aligned} \quad (5)$$

The matrix $[L]$ is simple to calculate analytically from Eq. (4). The matrix $[M]$ is straightforward to calculate using standard finite element shape functions for displacement measurements and strain-displacement relationships for strain and tilt measurements. For displacement measurements it is simply an identity matrix. Calculation of the derivatives for the $[G]$ matrix is less straightforward since u is an implicit function of θ through the Newton-Raphson iteration procedure. Following the approach presented by Xu et al. [13], this obstacle is overcome through application of the implicit function theorem, which allows $[G]$ to be expressed as

$$\begin{aligned} \frac{\partial u}{\partial \theta} &= [G] = - \left[\frac{\partial r(u, \theta)}{\partial u} \right]^{-1} \left[\frac{\partial r(u, \theta)}{\partial \theta} \right] \\ &= -[J_u]^{-1} [R] \end{aligned} \quad (6)$$

Since $[J_u]$ is already computed as part of the Newton-Raphson solution procedure, the only new calculation needed is the matrix $[R]$, containing the derivatives of Eq. (1) with respect to the constitutive model parameters. In some cases, such as for linear elasticity, this derivative can be computed analytically, though the derivation and implementation is quite tedious and error prone. For both purely physics-based models and for cases where the constitutive model is replaced or augmented with a deep learning model, the required derivatives can be computed using automatic differentiation (AD). For the examples shown in this paper reverse-mode AD was implemented using the PyTorch C++ library [2]. Unlike purely data-driven approaches, where AD is used to compute gradients of a scalar quantity (the loss function) with respect to a vector of parameters, in this physics-informed approach we require computation of the Jacobian relating one vector (the nodal residuals) with respect to a vector of parameters. This loses some of the computational efficiency of reverse-mode AD (i.e. back propagation). Nevertheless, reservoir mode AD is used for the analyses presented below, but further research is recommended to determine the most efficient way to implement AD to compute these derivatives.

Although the results shown below involve only single-process computations, this approach lends itself to MPI-parallel computations, which are expected to greatly speed up the process and be required for actual CO₂ storage site operations. For MPI-parallel finite element calculations there is no need to use AD to back propagate across MPI processes since the contributions of each process to $[R]$ can be computed independently and summed during global assembly just as is done with $[J_u]$. Although AD libraries capable of tracking derivatives across MPI processes now exist [1], it is possible that using such libraries could improve the efficiency of the reverse-mode AD algorithm used here. This is a

recommended area for further research. Also, because the nodal displacements are simply the sum of the incremental change occurring during each time step, Eqs. (5) and (6) can be applied to each time step and summed along with the displacements to compute the total gradient after all time steps to be used in training. Once the loss function and its gradients with respect to the constitutive model parameters have been calculated, a quasi-Newton optimization method can be used to solve the inverse problem for the constitutive model parameters that best fit the data.

For the demonstration problem presented below the finite element calculations were implemented in a C++ code wrapped with a Python interface. The optimization problem was then solved using the L-BFGS-B [5] optimization algorithm provided by the SciPy optimization library.

3. Results

3.1. Description of case study problem

A synthetic example problem was used to demonstrate the autonomous data integration approach presented above. This example consists of a simplified model of a GCS site. The model consists of a 20 m thick reservoir at a depth of 1200 m. The sealing formation is a 200 m thick unit. Shallower aquifers are represented by a single formation extending from the ground surface to the top of the sealing formation. Underlying the reservoir is a relatively stiff underlying formation extending 1000 m below the base of the reservoir. Table 1 lists the true elastic properties of each formation. The purpose of this paper is to describe the model and demonstrate its use on a scenario that is simplified from reality, but realistic in terms of the scale and geometry of the problem and the number and magnitude of measurements. For this reason we will limit the case study to homogeneous constitutive model parameters within each formation, and limit the constitutive model to isotropic linear elasticity.

As described in the introduction, one of the major motivations of this work is the observation that real geomaterials seldom behave in an isotropic linear elastic manner. This study should be seen as a step toward the development of field instrumentation and numerical modeling approaches that are able to characterize such complex rheology using in situ measurements. With that being said, there may be cases where modeling the complex behavior of subsurface systems using a simplified elastic model could be good enough to capture the coarse-grained response of the system. Even a viscoplastic material response can be well characterized with an elastic model if the loading rate is relatively steady and of modest magnitude, such as a gradual increase of the pressure in a GCS reservoir. Using an elastic model in this way amounts to fitting the tangent stiffness of the system under the loading direction it is experiencing. Such a model can be useful to extrapolate the behavior of the system under continued loading of the same nature. Under this scenario, using in situ instrumentation as proposed here would still offer a significant advantage over use of core and log

Formation	Depth Range	Young's Modulus	Poisson's Ratio	Number of Vertical Elements
Aquifer	0-1000 m	10 GPa	0.3	6
Cap Rock	1000-1200 m	35 GPa	0.28	8
Reservoir	1200-1220 m	20 GPa	0.2	5
Basement	1220-2220 m	70 GPa	0.23	6

Table 1: Four formations in model with their true elastic properties

measurements because the loading rates of the actual system are drastically different from those used in core and log measurements. This approach would not generalize well to changes in the nature of the system, such as depressurization.

Solving the pore pressure inversion problem is beyond the scope of this paper, so this study takes the pore pressure field as deterministic and well known. In practice, or course, this is not generally the case and the determination of the pore pressure field, along with the geomechanical state that is the focus of this paper, is one of the primary challenges of CO₂ storage site operation. The pore pressure in the case study problem is prescribed to be initially hydrostatic. The perturbation associated with injection modeled using a simple linear function of the radius from the injection well and is uniform across the vertical extent of the reservoir. The pressure in all regions outside of the reservoir remain in a hydrostatic condition. The center of the pressure plume is prescribed to increase linearly with time such that the perturbation above hydrostatic pressure is 10 MPa at five years of injection. The edge of the pressure plume is prescribed to be at 2.5 km from the injection well.

Figure 1 shows the size of the computational domain and mesh used for the calculations. The model represents a 1/4 symmetric model of a 3D storage reservoir. Zero normal displacement boundary conditions are specified on all except for the top surface, where a zero traction boundary condition is applied. All formations are assigned a uniform mass density of 2500 kg/m³ and gravitational loading is applied in the z-direction, which is downward. The model uses a structured hexahedral mesh with 20 elements in the lateral dimensions and 25 in the vertical direction. The number of elements used in the vertical direction for each formation is specified in Table (1).

To improve the conditioning of the optimization problem, in addition to scaling the measurement contributions to the loss function as done in Eq. (4), the constitutive parameters are also scaled to be approximately of order unity. Specifically, the Young's modulus was scaled by

$$\bar{E} = \frac{E}{E_o}. \quad (7)$$

For all calculations presented below E_o was chosen to be 100 GPa. Poisson's ratio was scaled by

$$\bar{\nu} = \frac{\nu}{0.5} \quad (8)$$

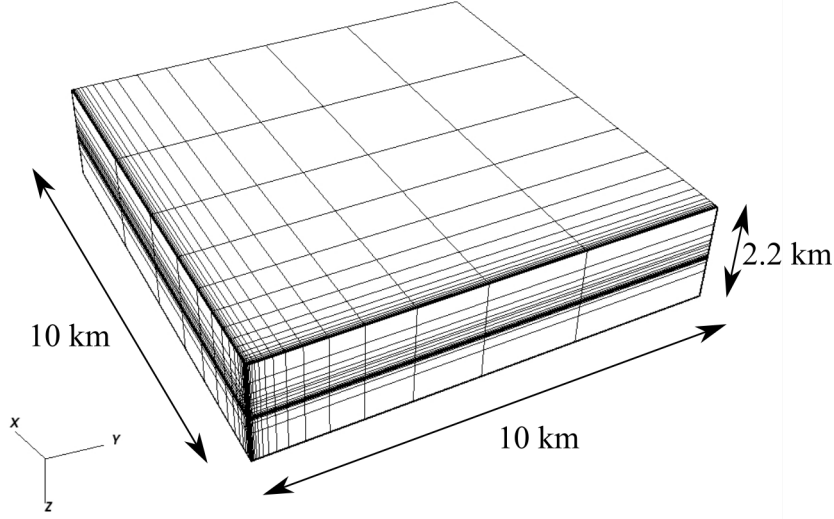


Figure 1: The size of the computational domain and mesh used

Using the bounds available in the L-BFGS-B algorithm, \bar{E} was constrained to be greater than 10^{-3} and less than 1.0, while $\bar{\nu}$ was constrained to be greater than 0.0 and less than 0.9. These bounds ensure positive definiteness of $[J_u]$ and stability of the solutions to linear systems containing it.

3.2. Geomechanical Measurements

A set of geomechanical monitoring measurements that would be technically feasible to implement were chosen to guide the autonomous data integration and inversion. Table 2, in the appendix, summarizes the location, type, and maximum value of each of the 33 measurements informing the inversion. One ground surface vertical displacement measurement is used in the inversion. This measurement is located at the injection well location and hence center of the pressure plume. Measurement such as this can be made using InSAR measurement. While InSAR surveys can provide a rich 2D data set, we have chosen to only use a single displacement measurement here because it is assumed that the spatial distribution of the surface displacement field is most sensitive to the pressure distribution, which we are taken as a given in this study. The magnitude of the ground surface displacement, however, is sensitive to the magnitude of the pressure perturbation and the elastic property field. For this reason we have chosen to use a single displacement point in the inversion since that will quantify the magnitude of the surface displacement. The strain

measurements with the smallest magnitude used in the analysis are in the base formation at the 3 km offset well, which have a magnitude of approximately 50 nano-strain ($n\epsilon$). Resolving strains of this magnitude would require strain meters grouted into the well bore, which have a resolution of approximately $10 n\epsilon$ [9]. All but one of the strains in the 1 km offset well have a magnitude of over $100 n\epsilon$, which according to Murdoch et al. [9] may be resolvable with strain meters cementing in the casing annulus, and are definitely within the range resolvable by strain meters temporarily clamped in the borehole. All strain measurements were scaled, according to Eq. (4), using a scale factor of $500 n\epsilon$, and the ground surface displacement was scaled by 5 mm.

3.3. Inversion Results

The inversion was performed by initializing each parameter to the middle of its range, 50 MPa for the Young's modulus of each formation and 0.25 for each Poisson's ratio ($\bar{E} = \bar{\nu} = 0.5$). As a test of the algorithm initially only a single time step of 5 years was used. Since the pressure perturbation in a self-similar over time, and the material is linear elastic, adding additional time steps would not add new information to the inversion. Figure 2 shows a plot of the loss function value as a function of the number of forward model runs. Note that the L-BFGS-B algorithm chooses a search direction based upon the gradient from a limited number (10 in this case) past iterations, and then performs an inexact line search in that direction, which required evaluating the forward model multiple times for each iterations. Since the forward model runs are the most computationally intensive part of the calculation all plots in this section are made with respect to the number of forward model evaluations rather than L-BFGS-B iterations.

Figure 3 shows a plot of the value of the Young's modulus and Poisson's ratio for the four formations as a function of the number of forward model runs. As the figure shows, each formation begins with the initial estimate of 50 GPa and 0.25. The loss function is most sensitive, by several orders of magnitude, to the reservoir elastic properties—particularly the Young's modulus. As a result of this the algorithm initially makes the largest changes in this parameters and after approximately 25 forward model evaluations this parameters has nearly converged to its true value. The next most sensitive parameter, despite its relative distance from the reservoir, is the Young's modulus of the shallow aquifer. This is most likely do to the thickness of this formation (1 km), which makes it have a large impact of the overall stiffness of the system. If a more realistic model were constructed with multiple overlying units it would be expected that the greater the distance from the reservoir the lower the sensitivity, but as this example shows, the thicker the formation the higher the sensitivity. More research needs to be done to evaluate how much information is lost when formations at a significant distance from the reservoir are lumped together into a single effective continuum. It seems likely that this could, as in this case, significantly simplify the problem perhaps without great cost in accuracy.

Figures 4 and 5 show comparisons between the true model and the inverted model in terms of the change in strain and stress fields induced by injection,

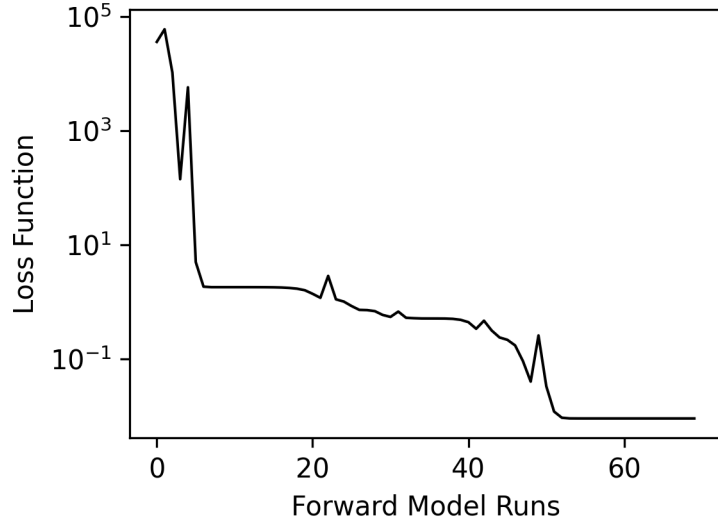


Figure 2: Plot of the loss function value versus number of forward model runs

respectively. Because the change in stress and strain values vary by several orders of magnitude throughout the problem domain and have both positive and negative, the changes are plotted in terms of the base-ten logarithm of the absolute value of the change of each component. The normal components of stress and strain in the y-direction are not shown since the problem is axisymmetric. The off-diagonal components of stress and strain are not shown because they are only a few kPa since the principal stress and strain directions are close to the x-, y-, and z-axes. In all cases the strain components are accurate to within three significant figures and the stress components are accurate to within less than one MPa.

4. Discussion

One of the key barriers for widespread commercial deployment of GCS is uncertainty about the ability to predict the hydromechanical response of the storage system over long periods of time. This uncertainty creates an elevation in perceived risk. This is particularly true of geomechanical aspects of the response because, unlike hydraulic aspects of the system, until recently there has been little or no data to inform and update geomechanical model predictions from the operational phase of a project. The primary diagnostics currently available are ground surface displacement using InSAR, changes in seismic attributes over time, and microseismic event locations and source mechanisms. While InSAR measurements have proved very insightful in a few cases [InSalah, Porotomo], many injection sites have failed to register any significant InSAR

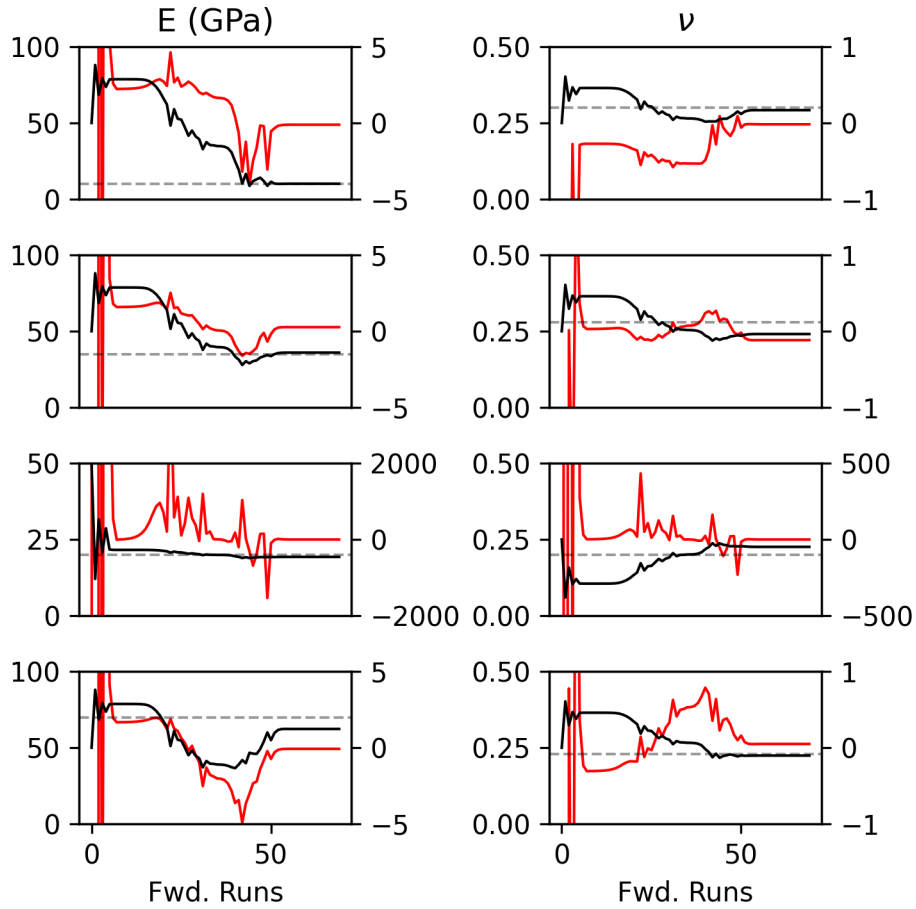


Figure 3: Plot of each of the nine inversion parameters versus number of forward model runs. The black curves are the parameter values, the dashed horizontal line is the true value, and the red lines are the gradients of the loss function with respect to the scaled version of each inversion parameter, which values plotted on the right-hand axis.

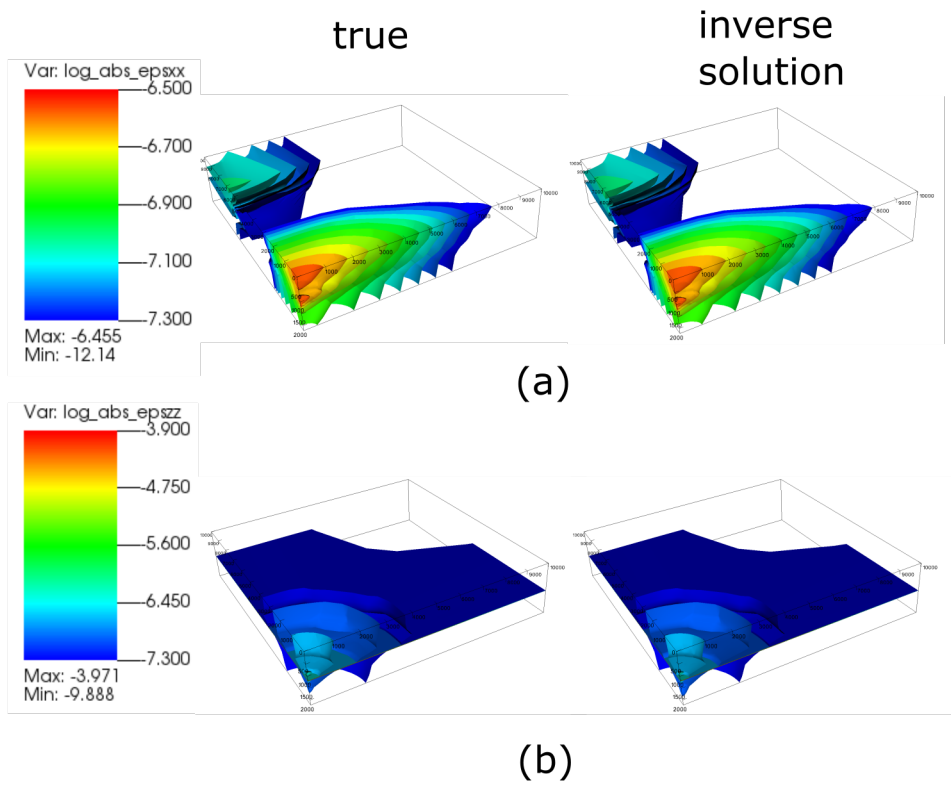


Figure 4: Comparison between the true strain solution between the true model and the inverse solution; (a) ϵ_{xx} component of strain; (b) ϵ_{zz} component of strain

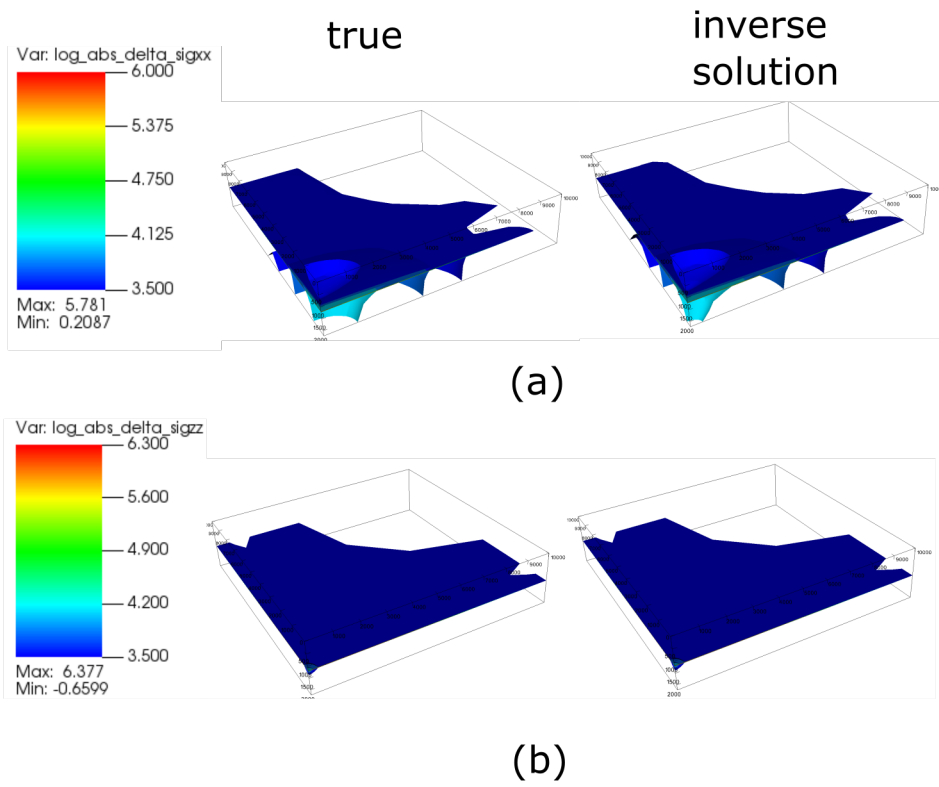


Figure 5: Comparison between the true stress solution between the true model and the inverse solution; (a) σ_{xx} component of strain; (b) σ_{zz} component of strain

signals above background. The surface expression of subsurface deformation is strongly influenced by the depth of injection and the distribution of geomechanical properties in the subsurface. Furthermore, many potential storage sites lie in areas where agricultural operations such as harvesting and plowing of fields, and seasonal aquifer draw down add noise that makes the injection-related signal difficult to detect.

Imaging changes in stress from surface-based seismic data can be very powerful in some cases, but it has several shortcomings. The first significant limitation is temporal resolution. Because of the large expense of repeated seismic surveys, time-lapsed seismic data is only likely to be available with years between acquisitions. Second, is the spatial resolution that is possible with surface-based seismic surveys. Because seismic attenuation increases substantially with frequency, deep seismic imaging relies on low frequency, long wavelength components, which necessarily limits the spatial resolution. A third major shortcoming of seismic imaging of stress is that even when significant changes in seismic attributes are detected, it is difficult to uniquely attribute the change to stress in a quantitative way. The primary reason for this is that the change in seismic attributes with stress varies strongly from formation to formation, and there is generally no way to calibrate a seismic attribute-to-stress model since stress changes generally cannot be measured directly. Laboratory tests on core samples can be used to measure change in acoustic velocity with stress, but it the differences in length scale and frequency that are involved generally make this solution less than satisfactory.

Currently the most common way of providing feedback to geomechanical models is using the locations, timing, and in some cases the source mechanisms from microseismic events. This is most commonly done to calibrate fracture propagation models in the petroleum industry. This approach is highly non unique and often overlooks the complex relationship between hydraulic fractures and microseismic events—specifically the fact that events can be triggered by a hydraulic fracture but at a distance from the fracture itself. More rigorous approaches have attempted to find relationships between in situ stress measurements and focal mechanisms [7, 6]. These studies have found that microseismic events often seem to be triggered at local heterogeneities in the stress field, which biases the image of the stress field if only this type of data is used. This is an important point to consider, as it is both a weakness of using microseismic events as a general stress field characterization tool, but it also highlights that microseismic events are extremely useful for identifying regions where the stress field is perturbed from larger-scale trends. Such locations may be critical to identify and understand but by their nature can be missed by stress measurement campaigns and coarse-grained geomechanical models.

Despite the shortcomings of the three methods discussed above, all of them have the potential to provide data that is informative for determining the geomechanical properties and state of a subsurface injection system under some circumstances. The strain measurements that are the focus of this paper are also not without their shortcomings. Rather than trying to decide which monitoring is best for informing a geomechanical analysis it will be better to evaluate

each method at a particular site using a detailed feasibility analysis and developing inversion algorithms that can use a wide variety of both redundant and complementary data.

4.1. Notes on the deformation field and sensitivity to elastic properties

The case study presented has a cap rock that is relatively stiff compared to the reservoir. This is a likely scenario in many locations since mature shale formations are often stiffer than high porosity sandstone formations. However, there are locations where primary seals would be composed of more compliant formations, such as immature shales and reservoirs may be composed of more stiff formations such as moderate porosity, well cemented sandstones or carbonate formations. Therefore, the trends described here only apply to storage complexes similar to the one considered here, where lateral strains due to expansion of the reservoir are constrained by the relatively stiff cap rock and underlying basement formation.

Along the vertical center line of the pressure plume the vertical strains are tensile inside the reservoir with a magnitude of approximately 250 micro-strain, and compressive outside the reservoir with a magnitude of a few micro-strains. The lateral strains are all tensile, which seems to be caused by the combined effect of lateral expansion of the reservoir and expansion due to the Poisson effect associated with compressive vertical strains outside of the reservoir. Because the overlying formations are much more compliant than the underlying formations there is also a bending deformation that occurs. Both the Poisson effects and the bending effects seem to dominate in this case since the lateral strains in the lower portion of the aquifer are larger in magnitude than those in the lower portion of the cap rock. As mentioned above, this is likely due to the constraint created by the relatively stiff cap rock formation at this location. This same trend occurs with the lateral strains at the 1 km offset monitoring well, where strains outside of but within several hundred meters the reservoir are on the order of several tenths of a micro-strain. The vertical strains at 1 km offset are larger in the lower portion of the relatively compliant aquifer formation than they are in the cap rock or base. The relative magnitude of the Young's modulus in each formation is a correlated more strongly than proximity to the pressurized reservoir. Lateral strains follow a similar trend suggesting that the Poisson effect is the stronger driver of lateral strains at this location than is lateral stretching of the formations outside of the reservoir.

4.2. Designing geomechanical monitoring approaches

The geomechanical monitoring system used in the case study problem presented here is only one of an infinite number of possible configurations, and is likely far from optimal. In an early draft of this study the inversion was attempted without strain monitoring in the injection well, and convergence to the true state of the system was much slower and less accurate. As described in the previous section, most of the strains outside of the reservoir and along the periphery of the pressure plume are caused by a combination of lateral stretching

of the reservoir and vertical compression caused by expansion of the reservoir. This latter effect seems to dominate in the case considered here with relatively stiff over- and underlying formations. The result is that the lateral strains in the overlying formations are from a combination of the Young's modulus and Poisson's ratio such that the inversion algorithm may have a hard time converging on the correct value of the Young's modulus, for example, because there are many pairs of Young's modulus and Poisson's ratio that fit the data almost as well as the true values. It was found that this effect was minimized by including strain values along the injection well where strains were larger in magnitude, and along the lower portion of each formation, in as close of proximity to the reservoir as possible, since strain magnitudes generally decay with distance from the reservoir. Though strains measured from an injection well are large and very informative, the injection of cold CO₂ in the same well bore is likely to create artifacts in the strain measurements that may be challenging to remove. Further investigation of these effects is warranted.

In the case study problem considered here, the true state of the system was able to be determined from only the injection well and two monitoring wells along a single radial direction. This was because the modeled system was radially symmetric. Furthermore, the number of inversion parameters was only nine because the subsurface system was lumped into a relatively small number of formations, each assumed to be homogeneous. This clearly represents an optimistic scenario. The approach presented here needs to be tested with subsurface systems with a higher degree of heterogeneity and complex rheology to evaluate how robust it is and what sort of monitoring strategies are required to constrain a more complex model.

Another aspect that needs to be considered in future evaluations of this approach is the effect of instrument noise. The very sensitive strain measurements envisioned in this study will also be sensitive to earth tides and in some cases human caused changes such as variation of fresh water aquifer levels. Such perturbations present both challenges and opportunities. The challenge they present is that these effects need to be either removed from the instrument responses or incorporated into the numerical model. The opportunity presented by these factors is that if they are incorporated into the numerical model they represent another forcing function beyond the fluid injection that can aid in resolving the system response more accurately[3].

Thus, in terms of computational time this approach is obviously not faster than existing approaches. However, given the potential for current approaches to significantly underestimate changes in stress and therefore geomechanical risk, comparison of the computational cost of the proposed approach with current deterministic forward modeling approaches is no appropriate. A more fair comparison is with two other approaches that rely on operational feedback to update the model over time: stochastic inversion approaches [8] and manual parameter updating [10]. A quantitative comparison of these approaches using the same data set would be very helpful to better determine the advantages and disadvantages of each. However, based on published results it appears that the stochastic inversion approach requires several orders of magnitude more forward

model runs than the deterministic inversion approach presented here. However, the stochastic approach has two distinct advantages over the approach presented here. First, for a Monte Carlo approach each model run is independent so they can be performed in parallel rather than sequentially. Second, the stochastic approach also can be used to estimate uncertainty in the inversion rather than only providing the best fit solution. A hybrid of these approaches may be best, where uncertainty can be estimated but the inversion can also be informed with gradient information. Manual parameter updating is time consuming in the sense that it requires an expert practitioner to manually evaluate data, gain an intuition for where the discrepancies in the model and observations are, and then determine, generally through trial and error, how to adjust the model parameters to fit the data. In this sense, even if the deterministic or stochastic inversion approaches are more computational expensive, they are likely to provide more timely results given that they do require minimal human interaction with observational data once the inversion has been set up. These inversion approaches are also able to find model parameters that describe the observational data very well but that expert intuition may fail to find.

5. Conclusion

This lack of substantial operational feedback on geomechanical predictions using existing approach adds to uncertainties from deficiencies in current geomechanical characterization approaches stemming from differences in loading rate, magnitude, and length scale between characterization methods and actual loading conditions. The model presented here demonstrates a proof of concept for leveraging recent developments in in situ deformation monitoring instrumentation to provide critical feedback to improve geomechanical modeling predictions over time. This has the potential to significantly improve upon the accuracy, level and timeliness of current approaches geomechanical modeling and risk estimation. While the approach suggested here requires additional costs to a site operator in the form of installation and operation of additional instrumentation, the approach also has the possibility of drastically reducing geomechanical uncertainties, which may justify their costs by allowing the system to be operated at a higher capacity, allowing the post-injection site care period to be shortened, and by alerting an operator to a hazardous condition early when the problem is small and manageable.

6. Acknowledgements

Funding for this research was provided as part of the Science-informed Machine learning to Accelerate Real Time decision making for Carbon Storage (SMART-CS) Initiative (edx.netl.doe.gov). Support for this initiative came from the U.S. DOE Office of Fossil Energy under DOE contract number DE-AC05-76RL01830. PNNL is operated by Battelle for the U.S. DOE under Contract DE-AC06-76RLO1830. This report was prepared as an account of

work sponsored by an agency of the United States Government. Neither the United States Government nor any agency thereof, nor any of their employees, makes any warranty, express or implied, or assumes any legal liability or responsibility for the accuracy, completeness, or usefulness of any information, apparatus, product, or process disclosed, or represents that its use would not infringe privately owned rights. Reference herein to any specific commercial product, process, or service by trade name, trademark, manufacturer, or otherwise does not necessarily constitute or imply its endorsement, recommendation, or favoring by the United States Government or any agency thereof. The views and opinions of authors expressed herein do not necessarily state or reflect those of the United States Government or any agency thereof.

We thank Dr. Grant Brohmhal, Dr. Srikanta Mishra, Dr. Josh White, Dr. Catherine Yonkofski, Dr. Diana Bacon, Dr. Alex Hanna, and Casie Davidson for their advice and encouragement.

References

- [1] Medipack. <https://github.com/SciCompKL/MeDiPack>.
- [2] Pytorch c++ api. <https://pytorch.org/cppdocs/>.
- [3] Matthew W. Becker and Thomas I. Coleman. Distributed acoustic sensing of strain at earth tide frequencies. *Sensors*, 19(9):1975, 2019. ISSN 1424-8220. doi: 10.3390/s19091975. URL <https://www.mdpi.com/1424-8220/19/9/1975/pdf>.
- [4] J. Burghardt. Geomechanical risk analysis for geologic carbon sequestration. In *51st U.S. Rock Mechanics/Geomechanics Symposium*, volume ARMA-2017-0478, 2017.
- [5] Richard H. Byrd, Peihuang Lu, Jorge Nocedal, and Ciyou Zhu. A limited memory algorithm for bound constrained optimization. *SIAM Journal on Scientific Computing*, 16(5):1190–1208, 1995. ISSN 1064-8275. doi: 10.1137/0916069. URL <http://epubs.siam.org/doi/10.1137/0916069?cookieSet=1>.
- [6] F. H. Cornet and Yin Jianmin. Analysis of induced seismicity for stress field determination and pore pressure mapping. *Pure and Applied Geophysics PAGEOPH*, 145(3-4):677–700, 1995. ISSN 0033-4553. doi: 10.1007/bf00879595.
- [7] F.H. Cornet and Ph. Julien. Stress determination from hydraulic test data and focal mechanisms of induced seismicity. *International Journal of Rock Mechanics and Mining Sciences & Geomechanics Abstracts*, 26(3-4):235–248, 1989. ISSN 0148-9062. doi: 10.1016/0148-9062(89)91973-6.
- [8] Alexander C. Hanna. *Stochastic Parameter Estimation of Poroelastic Processes Using Geomechanical Measurements*. Thesis, 2019.

- [9] Lawrence C. Murdoch, Leonid N. Germanovich, Scott J. Dewolf, Stephen M.J. Moysey, Alexander C. Hanna, Sihyun Kim, and Roger G. Duncan. Feasibility of using in situ deformation to monitor co2 storage. *International Journal of Greenhouse Gas Control*, 93:102853, 2020. ISSN 1750-5836. doi: 10.1016/j.ijggc.2019.102853.
- [10] Jonny Rutqvist, Pierre Jeanne, Patrick F. Dobson, Julio Garcia, Craig Hartline, Lawrence Hutchings, Ankit Singh, Donald W. Vasco, and Mark Walters. The northwest geysers egs demonstration project, california part 2: Modeling and interpretation. *Geothermics*, 63:120–138, 2016. ISSN 0375-6505. doi: 10.1016/j.geothermics.2015.08.002. URL <https://doi.org/10.1016/j.geothermics.2015.08.002>.
- [11] Hiroki Sone and Mark D. Zoback. Time-dependent deformation of shale gas reservoir rocks and its long-term effect on the in situ state of stress. *International Journal of Rock Mechanics and Mining Sciences*, 69:120–132, 2014. ISSN 1365-1609. doi: <http://dx.doi.org/10.1016/j.ijrmms.2014.04.002>. URL <http://www.sciencedirect.com/science/article/pii/S1365160914000896>.
- [12] Yunhui Tan, Shugang Wang, Margaretha Rijken, Kelly Hughes, Ivan Lim Chen Ning, Zhishuai Zhang, and Zijun Fang. Geomechanical template for distributed acoustic sensing strain patterns during hydraulic fracturing. *SPE Journal*, 26:1–12, 2021. doi: 10.2118/201627-PA.
- [13] Kailai Xu, Alexandre Tartakovsky, Jeffrey Burghardt, and Eric Darve. Learning viscoelasticity models from indirect data using deep neural networks. *Computer Methods in Applied Mechanics and Engineering*, 2021 (under revision). URL <https://arxiv.org/abs/2005.04384>.

Appendix

Measurement	Type	Formation	Depth (m)	Offset (m)	
1	vertical displacement	Aquifer	0	0	1.6 mm
2	east strain	Aquifer	980	0	312 $n\epsilon$
3	vertical strain	Aquifer	980	0	-502 $n\epsilon$
4	east strain	Cap Rock	1190	0	290 $n\epsilon$
5	vertical strain	Cap Rock	1190	0	-541 $n\epsilon$
6	east strain	Reservoir	1210	0	356 $n\epsilon$
7	vertical strain	Reservoir	1210	0	107 $\mu\epsilon$
8	east strain	Base	1230	0	241 $n\epsilon$
9	vertical strain	Base	1230	0	-322 $n\epsilon$
10	east strain	Aquifer	980	1000	213 $n\epsilon$
11	west strain	Aquifer	980	1000	158 $n\epsilon$
12	vertical strain	Aquifer	980	1000	-204 $n\epsilon$
13	east strain	Cap Rock	1190	1000	174 $n\epsilon$
14	west strain	Cap Rock	1190	1000	145 $n\epsilon$
15	vertical strain	Cap Rock	1190	1000	-137 $n\epsilon$
16	east strain	Reservoir	1210	1000	170 $n\epsilon$
17	west strain	Reservoir	1210	1000	144 $n\epsilon$
18	vertical strain	Reservoir	1210	1000	90 $\mu\epsilon$
19	east strain	Base	1230	1000	166 $n\epsilon$
20	west strain	Base	1230	1000	142 $n\epsilon$
21	vertical strain	Base	1230	1000	-98 $n\epsilon$
22	east strain	Aquifer	980	3000	135 $n\epsilon$
23	west strain	Aquifer	980	3000	711 $n\epsilon$
24	vertical strain	Aquifer	980	3000	-118 $n\epsilon$
25	east strain	Cap Rock	1190	3000	118 $n\epsilon$
26	west strain	Cap Rock	1190	3000	535 $n\epsilon$
27	vertical strain	Cap Rock	1190	3000	-88 $n\epsilon$
28	east strain	Reservoir	1210	3000	117 $n\epsilon$
29	west strain	Reservoir	1210	3000	52 $n\epsilon$
30	vertical strain	Reservoir	1210	3000	56 $\mu\epsilon$
31	east strain	Base	1230	3000	115 $n\epsilon$
32	west strain	Base	1230	3000	53 $n\epsilon$
33	vertical strain	Base	1230	3000	-62 $n\epsilon$

Table 2: Summary of measurement informing inversion